SF2A 2016
C. Reylé, J. Richard, L. Cambrésy, M. Deleuil, E. Pécontal, L. Tresse and I. Vauglin (eds)

SIMULATING THE LOCAL UNIVERSE

J. G. Sorce[1]

Abstract.
In the local Universe, cosmic structures can be observed down to very small scales, scales on which the standard cosmological model might fail. Such detailed observations have to be compared with simulations in order to verify the predictions of different cosmological models. However, the cosmic variance can obscure the tests. More precisely, comparisons on a one-to-one basis are feasible only with simulations that look like the local Universe. Constrained by observed positions and peculiar velocities of galaxies, the simulations presented here reproduce locally the three-dimensional distribution of matter. Within a sphere of radius 100 h^{-1} Mpc, the observed nearby Large and Small Scale Structure is simulated with an accuracy of a few megaparsecs. These simulations include our nearest cluster neighbor, Virgo, allowing a detailed study of its formation history. It follows that the Virgo cluster has had a quiet merging history within the last seven gigayears. In the near future, zoom-in hydrodynamical simulations of the later will permit deeper comparisons with observations.

Keywords: cosmology: large-scale structure of universe, galaxies: clusters: individual, methods: numerical, n-body simulations

1 Introduction

Cosmological simulations of structure formation rely on the cosmological principle which assumes the homogeneity of the Universe on large enough scales. The random nature of the primordial Gaussian perturbation field however implies that properties of patches of a few megaparsecs vary widely. To overcome this cosmic variance, statistical comparisons between observations and simulations to test cosmological models are based on large observational datasets (e.g. Stoughton et al. 2002; Abazajian et al. 2003, 2009) and large cosmological simulations (e.g., Klypin et al. 2011; Alimi et al. 2012; Prada et al. 2012; Angulo et al. 2012; Watson et al. 2014; Klypin et al. 2014; Skillman et al. 2014; Dubois et al. 2016). An alternative approach is to reduce the cosmic variance by focusing on the nearby Universe and by reproducing the local Large Scale Structure numerically.

This approach has two advantages: 1) the local Universe is without any doubt the best-observed volume of the Universe and as such allows very detailed comparisons with simulations down to the small scales; 2) a very large box size is not required to simulate our neighborhood, hence high resolutions required to study the smallest scales can be achieved without being overly time consuming. Still, while standard cosmological simulations are obtained straightforwardly from a random realization of the primordial perturbation field within a cosmological framework, local observational datasets are required as additional constraints in order to get simulations that resemble our neighborhood.

Generating constrained initial conditions consists in reconstructing first the density field today from sparse and noisy observational data of the local galaxies like positions and radial peculiar velocities (Kolatt et al. 1996; Kravtsov et al. 2002; Klypin et al. 2003; Sorce et al. 2014) or redshift catalogs (Heß et al. 2013). Second, the initial linear density field or initial conditions must be retrieved either backwards as in the POTENT reconstruction method (Dekel et al. 1990; Bertschinger et al. 1990; Nusser & Dekel 1992) or in the CLUES project* (Constrained Local Universe Simulations, Gottlöber et al. 2010; Yepes et al. 2014) with the Constrained Realizations technique (Hoffman & Ribak 1991; Ganon & Hoffman 1993) or forwards as recently proposed by Kitaura (2013); Heß et al. (2013); Jasche & Wandelt (2013); Wang et al. (2013). In the latter case, the initial

[1] Leibniz-Institut für Astrophysik, 14482 Potsdam, Germany
*http://www.clues-project.org/

field is sampled from a probability distribution function consisting of a Gaussian prior and a likelihood (see Wang et al. 2014, for a complete overview).

This paper uses the backward technique and focuses on using peculiar velocities as constraints. Indeed, although measuring peculiar velocities is challenging, such velocities are highly linear, correlated on large scales and excellent tracers of the underlying gravitational field as they account for both the baryonic and the dark matter. The results are presented as follows. In the second section, the methodology widely described in Sorce et al. (2014, 2016); Sorce (2015) is briefly reviewed. The third section compares the observed and the simulated local Large Scale Structure at redshift zero and presents the reduction of the cosmic variance using sets of random and constrained simulations. Before concluding, in the fourth section, the merging history of the dark matter halo unique candidate for the Virgo cluster is studied.

2 Methodology & Data

2.1 Radial peculiar velocity catalogs

The second generation observational catalog of radial peculiar velocities, built by the Cosmicflows[†] collaboration and used as constraints within the CLUES project is abundantly described in Tully et al. (2013). In short, 8,000 accurate galaxy peculiar velocities constitute this catalog. They are derived from distance measurements obtained mostly with the Tully-Fisher (Tully & Fisher 1977) and Fundamental Plane relations (Colless et al. 2001). Cepheids (Freedman et al. 2001), Tip of the Red Giant Branch (Lee et al. 1993), Surface Brightness Fluctuation (Tonry et al. 2001), supernovae of type Ia (Jha et al. 2007) and other miscellaneous methods provide the rest.

2.2 Techniques: grouping, minimization of biases, WF, CR, etc

The catalog undergoes a series of treatment to produce constrained initial conditions as reported in the following text:

• it is grouped to remove non-linear, virial motions (e.g. Tully 2015b,a) that would backfire when using the linear reconstruction method to produce the linear density field. More precisely, datapoints belonging to a single cluster are collapsed into one observational datapoint in the catalog.

• biases are minimized (Sorce 2015) within the catalog to erase the spurious infall on the local Volume observed in the reconstruction. Briefly, positions and peculiar velocities are corrected.

• the cosmic displacement field is reconstructed with the Wiener-Filter technique (linear minimal variance estimator abridged to WF, Zaroubi et al. 1995, 1999) applied to the catalog of constraints.

• the noisy radial peculiar velocity constraints are relocated at the positions of their progenitors via the reconstructed cosmic displacement field to ensure the proper location of the structures at z=0 (Doumler et al. 2013c,a,b) and they are replaced with their WF 3D reconstructions (Sorce et al. 2014).

• the Constrained Realization technique (schematically WF+Random field=CR, Hoffman & Ribak 1991, 1992) combines the modified observational peculiar velocities with a random realization to restore statistically the missing structures to produce constrained linear density fields.

• the density fields are rescaled to higher redshifts and possibly the resolution is increased by adding small scale features (with e.g. GINNUNGAGAP code[‡]) to complete the construction of constrained initial conditions.

2.3 Set of Constrained Simulations

A set of 25 constrained simulations with 512^3 particles and a box size of 500 h^{-1} Mpc are performed based on initial conditions obtained with this full process and the N-body code GADGET (Springel 2005). Fifteen of these simulations are based on different random realizations of Gaussian fields. They are called hereafter different-RR simulations. The remaining ten simulations share the same random large scale field but different small scale features have been added to increase the resolution (see Sorce et al. 2016, for a more detailed explanation). From now on, they are referred to the same-RR simulations. The two subsets allow us to evaluate to which extent the large and the small (non-linear and thus unconstrained) scales influence the evolution and formation history of the large scale structure and of the Virgo candidate studied further in this paper. Two simulations

[†] http://www.ipnl.in2p3.fr/projet/cosmicflows/

[‡] https://github.com/ginnungagapgroup/ginnungagap

with 1024^3 particles with the same box size have been run to check that results shown here are not affected by the mass resolution. Simulations are run within the framework of Planck cosmology (Ω_m=0.307, Ω_Λ=0.693, H_0=67.77, $\sigma_8 = 0.829$, Planck Collaboration et al. 2014). The starting redshift is z=60 and the force resolution is set to 25 h^{-1} kpc.

3 The local Large Scale Structure

3.1 Observations, Reconstructions and Simulations

To orientate similarly observations, reconstructions and simulations of the local Universe for comparison purposes, an observer is assumed to be at the center of the reconstructed and simulated boxes and the three supergalactic coordinates are defined similarly to observational ones. Before comparisons, a brief description of the local observed structures is a must. For that purpose, a simulation is drawn randomly from the set of 25 simulations and shown in Figure 1. Note that the choice of the simulation has no impact on the following discussion as simulations all reproduce the local Large Scale structure within a $\sim$200 h^{-1} Mpc radius area. While the left panel of Figure 1 presents the WF reconstructed linear density (contour) and velocity (arrows) fields in a 5 h^{-1} Mpc thick slice of the XY supergalactic plane, the right panel shows the randomly selected simulated non-linear density (contour) and velocity (arrow) fields[§] in the same slice. On top of the fields, red dots stand for galaxies from the 2MASS redshift catalog (Huchra et al. 2012) in a 10 h^{-1} Mpc thick slice. Several well-known structures and voids can be identified like Perseus-Pisces (PP), Shapley, Coma superclusters and the Sculptor void. In addition to the major structures and voids, the Zone of Avoidance (ZOA) due to our Milky-Way dust is marked highlighting the importance of the simulations over the reconstruction. While no reconstructed structures are visible beyond 50 h^{-1} Mpc from the center of the box due to a lack of information in the observed data, the simulated ZOA hosts structures, in particular connections between objects above and below the ZOA.

Comparing observations, reconstructions and simulations is not straightforward. There are some limitations involved: 1) the observed galaxy surveys are magnitude limited and suffer from the luminosity bias, the reconstruction presents only the linear fields and tends to the null field in absence of data or in presence of noisy data. Actually, these limitations highlight again the importance of the simulations: they give access not only to the formation history but also to the non-biased full (including non-linearities) fields of the local Universe.

Qualitative comparisons reveal a good agreement between the 2MASS redshift catalog, the reconstruction and the simulation on Figure 1. This agreement can be quantified with the cosmic web (e.g. gravitational tidal, displacement and velocity shear tensors, Hahn et al. 2007; Lavaux & Wandelt 2010; Hoffman et al. 2012). Focusing on the velocity shear tensor, its eigenvalues permit to distribute cells into knots, filaments, sheets and voids. It is thus straightforward to determine the environment of a galaxy in the cosmic web. With a null threshold and the definition used in Hoffman et al. (2012) for the velocity tensor, three negative eigenvalues correspond to a void while three positive values stand for a knot. Two negative and one positive values constitute a sheet while the opposite configuration reveals a filament. Observationally, filaments and sheets should host more or less the same large amount of galaxies ($\sim$ 35-45 %) while knots and voids should shelter only a small fraction of them ($\sim$ 10 %) (e.g. Forero-Romero & González 2015; Libeskind et al. 2012, who showed that the fractions are quasi independent of the threshold choice as long as it is reasonable). The results averaged over the fifteen different-RR constrained simulations give 6$\pm$1 % of the galaxies in knots, 35$\pm$2 % in filaments, 48$\pm$2 % in sheets and 10$\pm$1 % in voids. The galaxies are distributed as expected. In addition, the derivation of the standard deviations between the simulated and reconstructed velocity fields reveals that reconstructions and simulations agree at about 100-150 km s^{-1} (i.e. 2-3 h^{-1} Mpc, the linear theory threshold, in terms of displacement). From these comparisons, it can be concluded that the major attractors and voids of the local Universe are properly simulated.

3.2 Reduction of the cosmic variance

The primary goal of constrained simulations is to reduce cosmic variance to allow detailed comparisons between simulations and observations to test cosmological models. In the previous section, the simulations have been shown to resemble the local Universe implying a qualitative reduction of the cosmic variance. In this section,

[§]obtained with a cloud-in-cell scheme applied to the distribution of particles

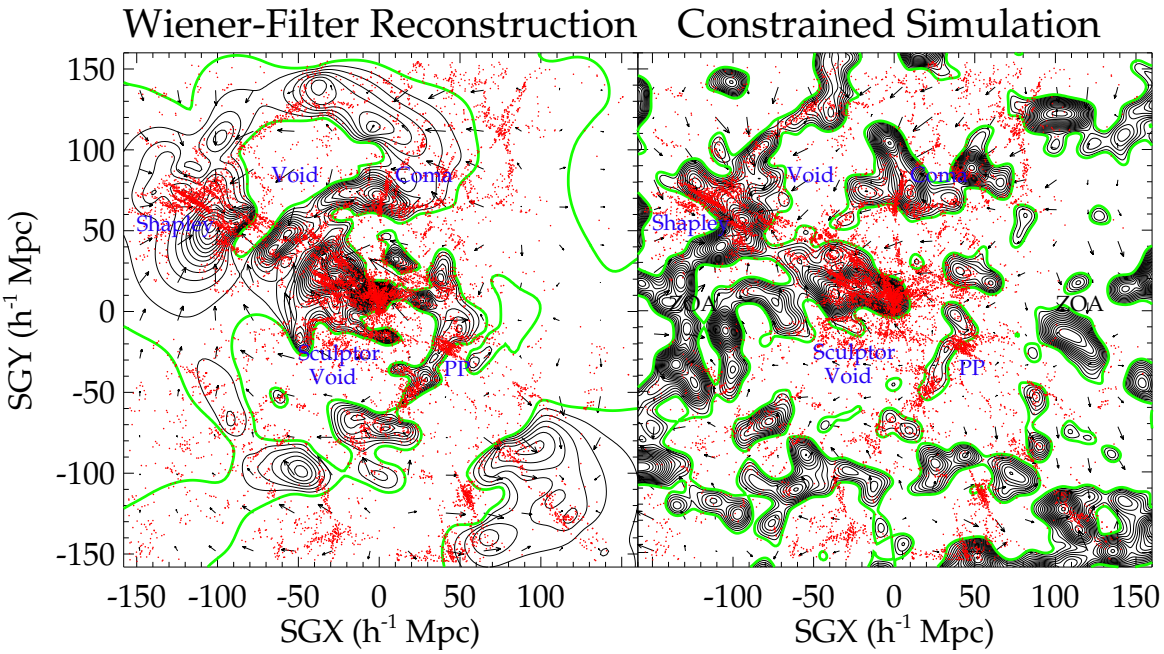

Fig. 1. XY supergalactic plane of the reconstructed overdensity (contours) and velocity fields of the local Universe obtained with the Wiener-Filter technique (left) and of the simulated density (contours) and velocity fields of one constrained simulations (right).The green color stands for the mean density. Arrows represent velocity fields. To facilitate the comparison, the simulation has been smoothed at 5 h^{-1} Mpc and the reconstruction at 2 h^{-1} Mpc which gives in both cases grid cells of $\sim$ 5 h^{-1} Mpc. Galaxies from the 2MASS redshift catalog, in a $\pm$ 5 h^{-1} Mpc thick slice, are superimposed as red dots. Structures, voids and flows of the local Universe are well recovered and simulated. A few of them are identified (blue names). While the Wiener-Filter reconstructs fairly well the local Universe in the center of the box, the simulation allows to go farther in distances and deeper into the Zone of Avoidance (ZOA) and, more importantly, it supplies the whole density field (including non-linearities).

the reduction of the cosmic variance is quantified between the different sets of simulations, i.e. constrained and random, to determine the constrained power of the method used. To this end, a cloud-in-cell scheme on a 512^3 grid is applied to the particle distributions of the simulations at z=0 with a subsequent Gaussian smoothing on a scale of 5 h^{-1} Mpc and a normalization by the mean density. A density-density plot (the density field of a first simulation versus the density field of a second simulation) is built from a cell-to-cell comparison of any pair of constrained simulations. The same is done with the random simulations. If the two simulations were identical all points would follow the 1:1 relation. The cosmic variance between two simulations can then be defined as the one-sigma, hereafter 1σ, scatter (or standard deviation) around this 1:1 relation. Mean and variance of the 1σ scatters are calculated for the 105 pairs of the 15 random simulations and those of the 15 constrained simulations as well as for the 45 pairs of the 10 constrained simulations sharing the same RR. In the left panel of Figure 2, this procedure gives three points (filled dark grey, black and light grey circles for each one of the simulation types: random, constrained, constrained sharing the same RR) with error bars at the x-axis value of 500 h^{-1} Mpc at z=0. The same is done in smaller sub-boxes of size 400, 300, 250 h^{-1} Mpc, etc, centered on the original box in order to measure the cosmic variance in the smaller central volumes where most of the observational data are, i.e. where they are the most effective.

The effect of the non-linear clustering is visible on small scales. As the system evolves and becomes more non-linear, a larger fraction of the sub-box is filled with low density regions (voids) rather than with high density regions (clusters). The densities of these nearly empty regions tend asymptotically to zero regardless of the initial field while that of high density regions, rising from small but positive differences in the initial field, are magnified. Consequently, the probability to compare a cell in a low density region with one in another low density region, with similar values, increases. This method limit explains the decrease of the 1σ scatters for sub-box smaller than 100 h^{-1} Mpc in the random simulations. Still the variance of these scatters increases because the probability to find a high density region in one of the pair simulation versus a low density region in the other simulation of the pair is non zero. The effect is (quasi-)inexistent for constrained simulations as

by construction structures (such as the Great Attractor and the Virgo cluster) are present close to the center of the box. The cosmic variance, defined as the 1σ scatter of cell-to-cell comparisons, is considerably reduced for constrained simulations, by a factor 2 to 3 on a scale of 5 h^{-1} Mpc in the inner part of the box, when compared to that of random simulations. In addition, the error bars of the constrained 1σ scatters are smaller by a factor at least 2 with respect to the random ones. The same procedure for the three components of the velocity field results in the same conclusion. As an example, taking a sub-box of 150 h^{-1} Mpc, the cosmic variance is decreased from 0.5 to 0.3 for the density fields normalized by the mean density at z=0 and from 150 to 50 km s^{-1} for the velocity fields. As a reference to assess the low values of the 1σ scatters and thus the small discrepancies between the constrained simulated velocity fields, one can consider the validity of the Wiener-Filter reconstructed velocity field which is ± [100-150] km s^{-1} (Sorce 2015).

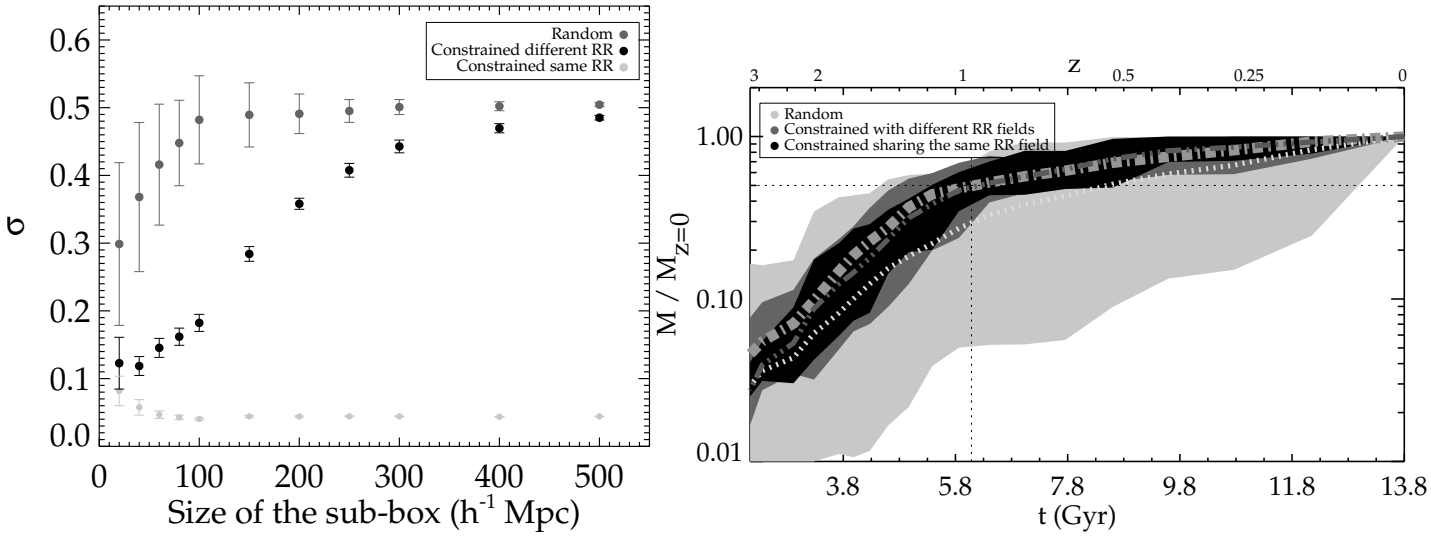

Fig. 2. Left: Mean (circles) and scatter (error bars) of one-sigma scatters (standard deviations) obtained with cell-to-cell comparisons carried out on pairs of density fields normalized by the mean density smoothed on a 5 h^{-1} Mpc scale at z=0. Scatters are given as a function of the sub-box size. Pairs are constituted of two random (dark grey), two constrained (black) and two constrained sharing the same random realization field (light grey) simulations. **Right:** Zones of possible merging histories obtained with 100 random halos sharing the same mass range as constrained halos (light grey), 15 Virgo halos from simulations built with different large scale random fields (dark grey) and 10 Virgo halos from simulations sharing the same large scale random field (black). The mean merging histories are plotted on top of the regions (dotted line for random, dot-dashed line for constrained with different large scale random fields and triple dot-dashed line for constrained sharing the same large scale random field). Masses at every redshift have been divided by the mass at redshift zero.

Since the variance between the different constrained simulations is relatively low, the local large scale environment is robustly simulated. Since this large scale environment has been suggested to play an essential role in the formation and evolution of local objects (e.g. Garrison-Kimmel et al. 2014), these constrained simulations are ideal to study local objects. The next subsection takes our nearest neighbor cluster, Virgo as an example.

3.3 An example: our nearest neighbor cluster, Virgo

For each simulation, a list of halos and their properties is established using Amiga Halo Finder (AHF, Knollmann & Knebe 2009) and the definition based on M_{200} (i.e the mass enclosed in a sphere with a mean density of 200 times the critical density of the Universe). The Virgo counterpart in each simulation is identified as the unique dark matter halo of reasonable mass (same order of magnitude) in spherical regions of 5 h^{-1} Mpc radius centered on the observed position of Virgo. The characteristics (position, mass, velocity) of the identified halos are within 10-20% of those of the observed Virgo.

Merging histories of the 25 Virgo halos are compared with those of 100 halos, selected randomly in the same mass range, at redshift zero, as the former. To this end, halos are split into three samples: the 15 Virgo halos from the different-RR simulations, the 10 Virgo halos from the same-RR simulations and the 100 randomly

selected halos. At a given redshift, minimum and maximum mass of any progenitor in a given sample are identified and the corresponding interval is plotted in the upper panel of Figure 2 once normalized by the mass at redshift zero. Therefore, these regions define the possible merging histories of the three different samples (dark grey, black and light grey respectively). For each sample, the mean merging history is plotted on top of the corresponding area with dot-dashed, triple dot-dashed and dotted lines.

Virgo halos present a smaller scatter in their merging histories than the 100 unconstrained randomly selected halos spanning over the same mass range (dark grey against light grey areas). At low redshifts, the variance of constrained halos' merging histories is decreased by a factor ~ 2 when compared to that of the merging histories of random halos. The 10 Virgo halos from the simulations sharing the same RR (black) present an even narrower range of merging histories as expected.

Moreover, random and Virgo halos do not share the same mean merging history: there is a break at redshift ~ 1 in the mean merging history of Virgo halos indicating that the accretion of material onto halos becomes smoother with time. At approximately the same redshift, Virgo halos have acquired about 50% of their redshift zero masses while the average random halo has gathered only about 30% of its mass. Namely, the large scale environment of the Virgo cluster considerably constrains its possible evolution.

4 Conclusions

Although the Universe is homogeneous on large scales, it is known not to be on the small scales rendering detailed one-to-one comparisons between observations and simulations difficult. A remedy to the problem consists in performing simulations that look like the local Universe to reduce the cosmic variance. Such simulations are produced with initial conditions constrained by observational data.

This paper presents and analyzes a set of such constrained simulations built with a refined technique applied to a catalog of local galaxy radial peculiar velocities. To measure efficiently the reduction of the cosmic variance, a set of 15 random simulations are compared to 15 constrained simulations. These simulations contain 512^3 particles within 500 h^{-1} Mpc. A check with two 1024^3-particles simulations showed that the results presented here are not affected by the number of particles. First, the general agreement of these simulations with our cosmic neighborhood is checked. Then the cosmic variance is shown to be reduced. To this end, a cloud-in-cell scheme is applied to the different simulated distribution of particles. The resulting fields undergo a 5 h^{-1} Mpc Gaussian smoothing and are normalized by their mean value. Defining the cosmic variance as the one-sigma scatter (or standard deviation) in density-density plots (field of a first simulation versus field of a second simulation), cell-to-cell comparisons between pairs of simulations of the same nature (random or constrained) are conducted. 1σ scatters obtained for the same nature pairs of simulations are averaged. Not only are these average 1σ scatters minimal when comparing the inner part of the simulated boxes, where most of the constraints are, but they are also smaller by a factor 2 to 3 with respect to those found for random simulations. The best constrained part of the simulations is the inner box within approximately 100 h^{-1} Mpc for the smallest (clusters) scales, the resemblance extends to 300 h^{-1} Mpc on larger scales (5 to a few tens of megaparsecs). This agreement meets expectations as the observational catalog used as constraints extends to 230 h^{-1} Mpc with 98% of the distance measurements within 160 h^{-1} Mpc and a median distance of 61 h^{-1} Mpc.

The variance between the different constrained simulations is relatively low implying that the local large scale environment is robustly simulated. Since this large scale environment has been suggested to play an essential role in the formation and evolution of local objects, these constrained simulations are ideal to study local objects. Our nearest neighbor cluster, Virgo constitutes such an example.

Applying a halo finder to the constrained simulations, a unique dark matter halo candidate for the Virgo cluster is identified in each one of the simulations. These halos share properties (position, velocity, mass) in common with the observed cluster at the 10-20% level. Studying their merging history and comparing it with that of random halos within the same mass range at redshift zero reveal that here again the cosmic variance is reduced by a factor 2 at low redshifts for the constrained halos: merging histories of randomly chosen halos of the same masses as the Virgo halos span over twice a larger range of possible histories. Interestingly, at around redshift 1, Virgo halos have already accreted 50% of their mass while an average random halo of the same mass has only accreted 30% of its mass. This suggests that the Virgo cluster has had a quiet merging history within the last seven gigayears compared to a random cluster of the same mass. This knowledge may be of extreme importance for observational analyses. In the near future, zoom-in hydrodynamical simulations of the Virgo candidates will allow deeper comparisons with observations.

The author gratefully acknowledges the Gauss Centre for Supercomputing e.V. (www.gauss-centre.eu) for providing computing time on the GCS Supercomputers SuperMUC at LRZ Munich and Jureca at JSC Juelich. JS acknowledges support from the Alexander von Humboldt Foundation and thanks her collaborators.

References

Abazajian, K., Adelman-McCarthy, J. K., Agüeros, M. A., et al. 2003, AJ, 126, 2081
Abazajian, K. N., Adelman-McCarthy, J. K., Agüeros, M. A., et al. 2009, ApJS, 182, 543
Alimi, J.-M., Bouillot, V., Rasera, Y., et al. 2012, ArXiv e-prints: 1206.2838
Angulo, R. E., , V., White, S. D. M., et al. 2012, MNRAS, 426, 2046
Bertschinger, E., Dekel, A., Faber, S. M., Dressler, A., & Burstein, D. 1990, ApJ, 364, 370
Colless, M., Saglia, R. P., Burstein, D., et al. 2001, MNRAS, 321, 277
Dekel, A., Bertschinger, E., & Faber, S. M. 1990, ApJ, 364, 349
Doumler, T., Courtois, H., Gottlöber, S., & Hoffman, Y. 2013a, MNRAS, 430, 902
Doumler, T., Gottlöber, S., Hoffman, Y., & Courtois, H. 2013b, MNRAS, 430, 912
Doumler, T., Hoffman, Y., Courtois, H., & Gottlöber, S. 2013c, MNRAS, 430, 888
Dubois, Y., Peirani, S., Pichon, C., et al. 2016, MNRAS
Forero-Romero, J. E. & González, R. 2015, ApJ, 799, 45
Freedman, W. L., Madore, B. F., Gibson, B. K., et al. 2001, ApJ, 553, 47
Ganon, G. & Hoffman, Y. 1993, ApJ, 415, L5
Garrison-Kimmel, S., Boylan-Kolchin, M., Bullock, J. S., & Lee, K. 2014, MNRAS, 438, 2578
Gottlöber, S., Hoffman, Y., & Yepes, G. 2010, ArXiv e-prints: 1005.2687
Hahn, O., Carollo, C. M., Porciani, C., & Dekel, A. 2007, MNRAS, 381, 41
Heß, S., Kitaura, F.-S., & Gottlöber, S. 2013, MNRAS, 435, 2065
Hoffman, Y., Metuki, O., Yepes, G., et al. 2012, MNRAS, 425, 2049
Hoffman, Y. & Ribak, E. 1991, ApJ, 380, L5
Hoffman, Y. & Ribak, E. 1992, ApJ, 384, 448
Huchra, J. P., Macri, L. M., Masters, K. L., et al. 2012, ApJS, 199, 26
Jasche, J. & Wandelt, B. D. 2013, MNRAS, 432, 894
Jha, S., Riess, A. G., & Kirshner, R. P. 2007, ApJ, 659, 122
Kitaura, F.-S. 2013, MNRAS, 429, L84
Klypin, A., Hoffman, Y., Kravtsov, A. V., & Gottlöber, S. 2003, ApJ, 596, 19
Klypin, A., Yepes, G., Gottlöber, S., Prada, F., & Hess, S. 2014, ArXiv e-prints: 1411.4001
Klypin, A. A., Trujillo-Gomez, S., & Primack, J. 2011, ApJ, 740, 102
Knollmann, S. R. & Knebe, A. 2009, ApJS, 182, 608
Kolatt, T., Dekel, A., Ganon, G., & Willick, J. A. 1996, ApJ, 458, 419
Kravtsov, A. V., Klypin, A., & Hoffman, Y. 2002, ApJ, 571, 563
Lavaux, G. & Wandelt, B. D. 2010, MNRAS, 403, 1392
Lee, M. G., Freedman, W. L., & Madore, B. F. 1993, ApJ, 417, 553
Libeskind, N. I., Hoffman, Y., Knebe, A., et al. 2012, MNRAS, 421, L137
Nusser, A. & Dekel, A. 1992, ApJ, 391, 443
Planck Collaboration, Ade, P. A. R., Aghanim, N., et al. 2014, A&A, 571, A16
Prada, F., Klypin, A. A., Cuesta, A. J., Betancort-Rijo, J. E., & Primack, J. 2012, MNRAS, 423, 3018
Skillman, S. W., Warren, M. S., Turk, M. J., et al. 2014, ArXiv e-prints: 1407.2600
Sorce, J. G. 2015, MNRAS, 450, 2644
Sorce, J. G., Courtois, H. M., Gottlöber, S., Hoffman, Y., & Tully, R. B. 2014, MNRAS, 437, 3586
Sorce, J. G., Gottlöber, S., Yepes, G., et al. 2016, MNRAS, 455, 2078
Springel, V. 2005, MNRAS, 364, 1105
Stoughton, C., Lupton, R. H., Bernardi, M., et al. 2002, AJ, 123, 485
Tonry, J. L., Dressler, A., Blakeslee, J. P., et al. 2001, ApJ, 546, 681
Tully, R. B. 2015a, AJ, 149, 54
Tully, R. B. 2015b, AJ, 149, 171
Tully, R. B., Courtois, H. M., Dolphin, A. E., et al. 2013, AJ, 146, 86

Tully, R. B. & Fisher, J. R. 1977, A&A, 54, 661
Wang, H., Mo, H. J., Yang, X., Jing, Y. P., & Lin, W. P. 2014, ApJ, 794, 94
Wang, H., Mo, H. J., Yang, X., & van den Bosch, F. C. 2013, ApJ, 772, 63
Watson, W. A., Iliev, I. T., Diego, J. M., et al. 2014, MNRAS, 437, 3776
Yepes, G., Gottlöber, S., & Hoffman, Y. 2014, New Astr. Rev., 58, 1
Zaroubi, S., Hoffman, Y., & Dekel, A. 1999, ApJ, 520, 413
Zaroubi, S., Hoffman, Y., Fisher, K. B., & Lahav, O. 1995, ApJ, 449, 446